High optical quality single crystal phase wurtzite and zincblende InP nanowires

2013 Nanotechnology 24 115705

(http://iopscience.iop.org/0957-4484/24/11/115705)

Nanotechnology **24** (2013) 115705 (6pp) doi:10.1088/0957-4484/24/11/115705

High optical quality single crystal phase wurtzite and zincblende InP nanowires

Thuy T T Vu[1,4], Tilman Zehender[1,4], Marcel A Verheijen[1,2], Sébastien R Plissard[1], George W G Immink[2], Jos E M Haverkort[1] and Erik P A M Bakkers[1,3]

[1] Eindhoven University of Technology, PO Box 513, 5600 MB Eindhoven, The Netherlands
[2] Philips Innovation Services, High Tech Campus 11, 5656AE Eindhoven, The Netherlands
[3] Kavli Institute of Nanoscience, Delft University of Technology, 2600 GA Delft, The Netherlands

E-mail: t.t.t.vu@tue.nl

Received 18 November 2012, in final form 25 January 2013
Published 1 March 2013
Online at stacks.iop.org/Nano/24/115705

Abstract
We report single crystal phase and non-tapered wurtzite (WZ) and zincblende twinning superlattice (ZB TSL) InP nanowires (NWs). The NWs are grown in a metalorganic vapor phase epitaxy (MOVPE) reactor using the vapor–liquid–solid (VLS) mechanism and *in situ* etching with HCl at a high growth temperature. Our stacking fault-free WZ and ZB TSL NWs allow access to the fundamental properties of both NW crystal structures, whose optical and electronic behaviors are often screened by polytypism or incorporated impurities. The WZ NWs show no acceptor-related emission, implying that the VLS-grown NW is almost free of impurities due to sidewall removal by HCl. They only emit light at the free exciton (1.491 eV) and the donor bound exciton transition (1.4855 eV). The ZB NWs exhibit a photoluminescence spectrum being unaffected by the twinning planes. Surprisingly, the acceptor-related emission in the ZB NWs can be almost completely removed by etching away the impurity-contaminated sidewall grown via a vapor–solid mechanism.

S Online supplementary data available from stacks.iop.org/Nano/24/115705/mmedia

(Some figures may appear in colour only in the online journal)

1. Introduction

Semiconductor nanowires (NWs) have been extensively studied because of their fascinating optical and electronic properties. They are recognized as promising candidates for future applications, including NW quantum bits [1, 2], the realization of Majorana's fermion [3], single photon detection [4] and next generation photovoltaic cells [5–8]. For a device, such as a NW solar cell, many requirements should be simultaneously met, including a perfect crystal phase, a low surface recombination velocity, the absence of unintentional sidewall growth and very low residual doping levels [5–8]. From a more fundamental point of view, the question arises whether the vapor–liquid–solid (VLS) growth mechanism allows the control of the NW growth down to the atomic scale, yielding the 'perfect NW'. In this paper, we will take a step towards this goal by demonstrating both purely wurtzite [9–11] (WZ) and purely zincblende (ZB) crystal phase ⟨111⟩ InP NWs grown by MOVPE in which the contamination by residual impurities has been almost completely removed.

Unintentional radial vapor–solid (VS) growth during VLS growth gives sidewall growth that not only leads to unwanted NW-tapering, but the low MOVPE nanowire growth temperature presumably also results in high impurity incorporation in the NW-shell [12, 13]. Thus, as a first step towards a high optical quality NW, the growth on the sidewall of NWs should be eliminated to avoid broadened bandgap-related photoluminescence (PL) and a degraded PL efficiency at room temperature. In this paper we built upon the approach of Borgström *et al* [13] by using *in situ* etching and surface passivation with HCl to prevent uncontrolled sidewall growth around the InP NW.

[4] These authors contributed equally.

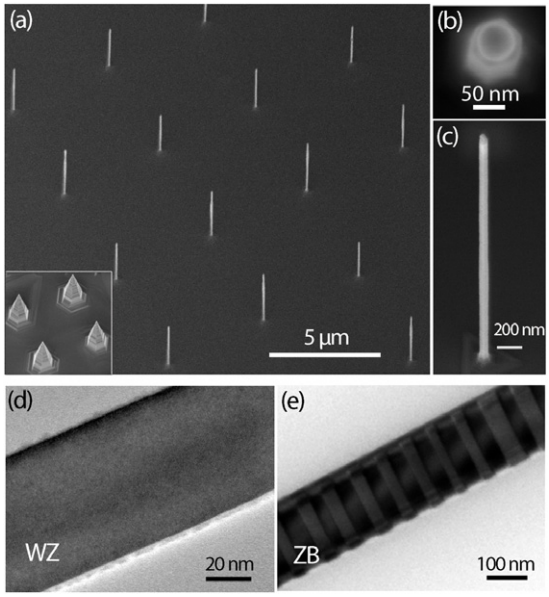

Figure 1. (a–c) SEM images of a nanowire array grown at 540 °C using *in situ* etching with HCl to suppress sidewall growth: (a) large-area view, (b) top-view and (c) zoom-in images. Inset of (a) shows NWs grown under identical growth conditions but without using HCl. (d,e) TEM images of a stacking fault-free WZ InP nanowire and a InP ZB twinning superlattice grown by using 20 nm and 80 nm Au catalyst nanoparticles, respectively. Imaging was performed along the $\langle 2\bar{1}\bar{1}0\rangle$ and $\langle 011\rangle$ zone axes, respectively.

Growth of III–V NWs using the vapor–liquid–solid (VLS) mechanism often results in polytypism with a random distribution of zincblende (ZB) and wurtzite (WZ) segments. Band structure differences between the two can lead to electron (hole) trapping in the ZB (WZ) segment [14, 15] and excess carrier scattering at stacking faults [16, 17]. These effects strongly degrade the NW optical and electronic properties as compared to a single crystal phase NW. As a second important step towards a high optical quality NW, *in situ* etching with HCl enables us to increase the conventional InP VLS growth temperature of about 420 °C into the range of 500–540 °C without suffering from unintentional sidewall growth. In this paper, we will show that the increased VLS growth temperature is a key to promoting purely WZ crystal phase NWs for small NW diameter [18, 19]. We show that both ZB twinning superlattices [20] (TSL) and pure WZ InP NWs are achieved with exactly the same growth conditions for different NW diameter.

As a third important step towards a high optical quality NW, we study the residual impurities within *in situ* etched NWs. It is important to note that the residual impurity incorporation is much more clearly visible in the PL spectra of pure crystal phase NWs. A high VLS growth temperature is expected to also be beneficial [12] for reducing the residual impurity incorporation within the NW core. We study the impurity incorporation by performing μ-PL measurements on single NWs at very low excitation density to highlight impurity-related PL. The μ-PL measurements are performed in direct correlation with transmission electron microscopy (TEM) to be able to unambiguously attribute the different PL peaks [21]. By this approach, we are able to resolve different excitonic emission lines and almost suppress the acceptor-related emission, which is probably the result of carbon incorporation [13, 22] in MOVPE-grown NWs. We finally measured a temperature-dependent series of the PL efficiency and observed an improvement at room temperature due to the reduction of the impurity incorporation. The suppression of the surface recombination with a suitable shell is beyond the scope of the present paper.

2. Experiments

Figure 1 shows scanning electron microscope (SEM) images of the InP NW sample grown at 540 °C on a $\langle 111\rangle$B InP substrate in an Aixtron 200 MOVPE system by using a 25 nm Au catalyst nanoparticle array and employing *in situ* etching with HCl. The NW-array displays uniform growth rate and the NWs show almost no tapering as compared to the pyramid-shaped NWs grown without HCl (inset of figure 1(a)). Similar results on *in situ* etching have been reported by Borgström *et al* [13]. Top-view and 30° tilted-view SEM images show that these NWs have a hexagonal cross-section with a diameter of about 60 nm and a length of 3 μm (figures 1(b) and (c)).

TEM images of stacking fault-free WZ and ZB TSL NWs grown by 20 nm and 80 nm Au seeds are presented in figures 1(d) and (e), respectively. For this study, NWs are dispersed randomly on transmission electron microscopy (TEM) grids for the direct correlation between PL measurements and the crystalline structure of the same single NWs [21]. For Au colloid catalyst sizes below 20 nm, we realize WZ InP NWs without any stacking fault with our growth conditions. When the catalyst particle diameter increases up to 50 nm, ZB TSL InP NWs are grown. Until now, the formation and control of both WZ and ZB TSL by using temperature and diameter has been reported for InAs and GaAs NWs [18, 19, 23]. InP has an optical bandgap which is near ideal for use in single-junction photovoltaics and also a much lower surface recombination velocity than GaAs [24]. So far, WZ InP NWs were realized by optimizing growth conditions such as growth temperature, nanowire diameter and V–III ratios [10, 25–29] or by using dopants [11]. The ZB TSL InP NWs, however, were mainly realized by Zn doping [20]. The present undoped WZ and ZB TSLs grown simultaneously at a very high temperature of 540 °C therefore provide useful input to a more complete understanding of InP NW growth and crystal structure formation. Our pure WZ and ZB TSL NWs allow us to access the fundamental properties of both InP crystal structure NWs, whose optical and electronic behaviors are often screened by stacking faults, polytypism, and intentional or unintentional impurity incorporation in the NW shell. In the following we will mainly focus on the optical and structural properties of these NWs by using μ-PL, TEM and PL-efficiency measurements.

3. High optical quality single crystal phase wurtzite and zincblende InP nanowires

Correlated μ-PL and TEM images of the same NW are presented in figure 2. TEM studies show that the studied InP NW grown from a 20 nm Au particle has a diameter of about 70 nm and a length of 1.7 μm. A careful HRTEM examination along the whole length of the NW indicates that it is free of any stacking faults or ZB insertions. The power-dependent μ-PL at 4 K of this NW reveals interesting spectra when we reduce the excitation density down to 0.25 W cm^{-2}, which is two orders of magnitude lower than the excitation density where the crystal phase quantum dots are studied [30] (~20–1000 W cm^{-2}), and ten times lower than the PL studies of the stacking fault-free WZ InP NW grown using sulfur reported in [11] and grown on $SrTiO_3$(001) substrate [26]. The low excitation power PL measurement allows us to observe the near-gap PL, which is well known for high-quality bulk-type semiconductors [31]. At the lowest excitation powers (0.25–0.8 W cm^{-2}), a peak is observed at 1.4855 eV, labeled (B) in the inset, with a FWHM of 1.5 meV. This is most probably the bound exciton (D^0, X) and/or the neutral donor recombination with a free hole (D^0, h) [11]. It is however important to note that no additional peaks, e.g. no donor–acceptor (D^0–A^0) or electron-acceptor (e–A^0)-related recombination, were observed, indicating that we realized almost no impurity incorporation due to the combination of HCl *in situ* etching and the high-temperature growth resulting in high-quality WZ NWs. The spectral line centered at 1.491 eV (dashed line in figure 2(d)) with a full-width at half-maximum of about 2 meV corresponds to free exciton recombination (peak (A) in the inset of figure 2). This free exciton recombination peak becomes pronounced at slightly higher excitation powers and dominates the PL spectra at powers higher than 2.5 W cm^{-2}. The free exciton PL peak gradually broadens and turns into free electron–hole recombination when the excitation density further increases and band filling appears [32, 33]. The observed PL spectra are essentially different from the PL spectra observed in WZ NW with ZB stacking faults, where the electrons and holes are trapped and then recombine radiatively at a lower energy, resulting in a broad emission in the region between the ZB and WZ bandgap energies (1.42–1.49 eV) [30, 33].

Importantly, other NWs of this sample yield similar results. PL peak positions and linewidths of five different NWs (see supplementary information figure S1a available at stacks.iop.org/Nano/24/115705/mmedia) are very consistent. We are therefore able to unambiguously determine the bandgap energy of the WZ InP to be at about $E_g = 1.491$ eV, which is close to the value reported [10, 11, 35]. These high-quality WZ NWs have potential for NW devices which require a single WZ crystal phase and low impurity contamination. At an excitation density exceeding 80 W cm^{-2}, we observe heating effects resulting from the low heat conductivity of the carbon film. The PL redshifts, broadens and decreases in intensity [21].

The direct correlation between the structural and the optical properties of a ZB NW is presented in figure 3. The

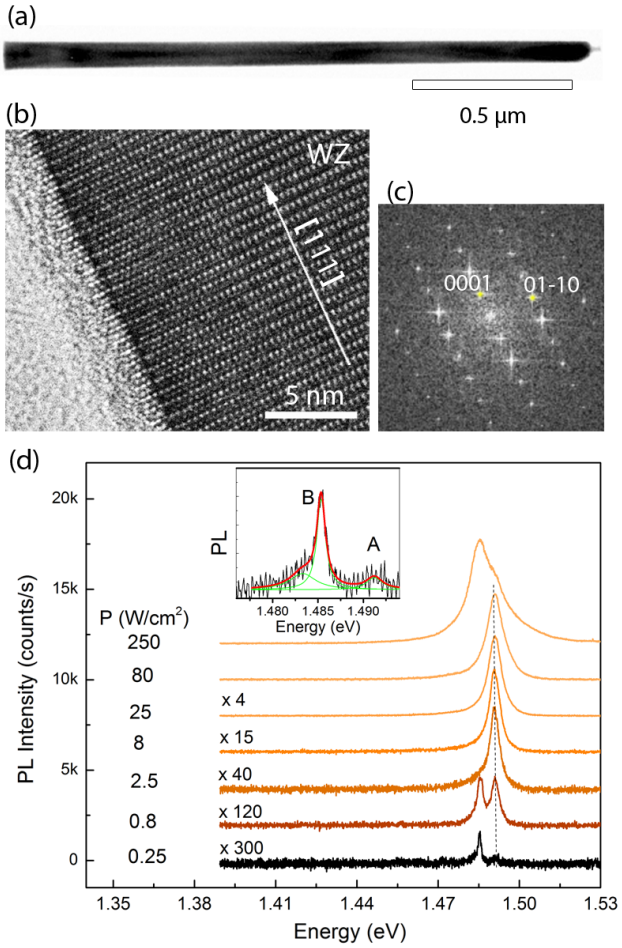

Figure 2. Direct correlation of the structural and optical properties of a pure WZ InP nanowire. (a), (b) and (c) TEM, HRTEM images along the $\langle 2\bar{1}\bar{1}0 \rangle$ zone axis, and associated FFT image. (d) Micro-PL-spectra of the same nanowire measured at excitation densities in the range 0.25–250 W cm^{-2} at 4 K. The inset shows the expanded bandgap-related PL at 0.25 W cm^{-2}.

TEM image shows a NW of about 200 nm in diameter and 3.5 μm in length containing many twins. A twin plane is defined as a mirror plane between two segments which are mutually rotated by 60°(figure 3(b)) [20]. Different from the growth with 20 nm Au catalyst nanoparticles, the 80 nm Au nanoparticles result in a ZB twinning superlattice (TSL), with a segment length between two twin boundaries of roughly 30 nm at the top part of the NW. At one third measured from the bottom of the NW, however, the twin-plane density increases. Again, no tapering effect is observed for this NW, showing that the *in situ* etching with HCl is effective. The μ-PL study on this NW presented in figure 3(d) shows two major peaks at 1.414 and 1.38 eV at low excitation powers. The first peak (FWHM = 6 meV, at 0.25 W cm^{-2}) is bandgap related and is at about 4 meV below the free exciton line observed in bulk [31]. The second peak, at 35 meV below the first peak, is attributed to either an acceptor-related transition [36] and/or the type II transition [30, 33] at the interface between WZ and ZB segments. The type II emission from twin planes (monolayers of WZ) would be very close to the bandgap-related transition from ZB InP (~1 meV below,

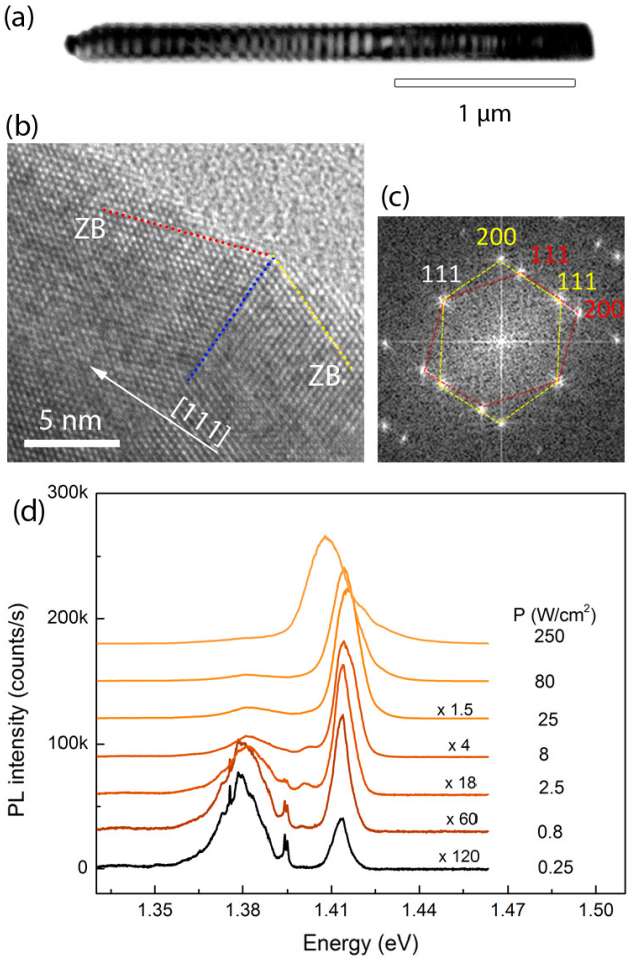

Figure 3. Direct correlation of the structural and the optical properties of a ZB twinning superlattice InP nanowire. (a), (b) and (c) TEM, HRTEM images along the ⟨011⟩ zone axis of a small area, and associated FFT image. (d) Corresponding micro-PL-spectra of the same nanowires measured at various excitation densities in the range of 0.25–250 W cm^{-2} at 4 K.

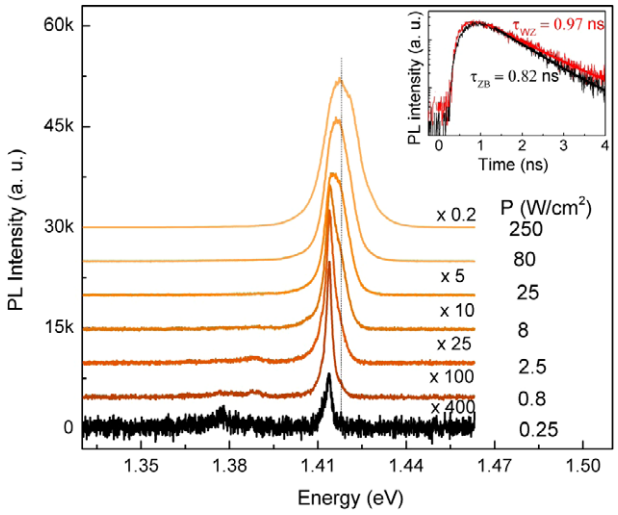

Figure 4. Micro-PL-spectra of an etched ZB twinning superlattice InP nanowire measured at various excitation densities in the range of 0.25–250 W cm^{-2} at 4 K. The inset shows the PL lifetime of the etched ZB nanowire in comparison with a pure WZ InP nanowire.

as predicted by Zhang *et al* [37]) and is not clearly observed in our data. Since we do not observe any WZ segment (consisting of 2 or more sequential twin planes) in this NW from HRTEM images, this peak can be unambiguously attributed to the D^0–A^0 and e–A^0 transitions. This observation implies that we have incorporated impurities in the ZB wires, but not in the WZ wires, while they were simultaneously grown in the same run. This point will be discussed below.

We notice two important differences between the PL of WZ and ZB NWs: (1) pure WZ NWs have a narrow and consistent PL peak while the bandgap peak of ZB TSL NWs is more broadened and varies slightly from NW to NW (supplementary information figure S1(b) available at stacks.iop.org/Nano/24/115705/mmedia). (2) The ZB NWs show pronounced acceptor-related impurity peaks, which do not appear in PL spectra of WZ NWs grown in the same run. This interesting phenomenon can be explained if we carefully examine the sidewall of the ZB NW in the TEM image. It is remarkable that the ZB NW has flat side facets instead of the saw-tooth facet morphology consisting of alternating {111}A and {111}B facets, which is essential for the creation of ZB TSL NWs [20]. The flat facets are explained by the overgrowth of the {111} side facets to form flat and stable {110} sidewalls [38]. Radial growth, at these high temperatures, is expected to be fast because of the re-entrant corners, which are at the concave positions where the {111}A and {111}B facets meet. When these corners have grown out, the growth rate decreases and is balanced by the *in situ* etching by HCl vapor [13]. The re-entrant corners are visible at the top part of the nanowire where they are not completely overgrown [38], as seen in figure 3(a) and figure S3(c) of the supplementary information (available at stacks.iop.org/Nano/24/115705/mmedia).

We found that sidewalls have dramatic consequences for the NW optical properties, which is shown by etching the NWs with piranha to remove the thin sidewall layer (see supplementary information available at stacks.iop.org/Nano/24/115705/mmediafor the details). The power dependence PL spectra of a ZB NW after piranha etching are presented in figure 4. We directly observe that the donor–acceptor (D^0–A^0) or electron-acceptor (e–A^0) peaks at 1.38 eV have been completely eliminated and the PL linewidth becomes as narrow as 2.5 meV. Similar to the WZ NWs, the etched ZB TSL NW shows only one free exciton feature at 1.418 eV, which becomes pronounced at high excitation power (dashed line in figure 4), and an impurity bound exciton line at 1.414 eV, respectively [31]. This interesting phenomenon shows that the core of the ZB TSL InP NW has a bulk-like PL spectrum which is not affected by the twinning planes.

The very high optical quality of both the WZ and the sidewall-etched ZB NW clearly indicates that the core NW, axially grown by the VLS mechanism, has excellent structural quality and contains almost no impurity contamination. The VS sidewall growth, in contrast, is highly contaminated by impurity incorporation even at a relatively high temperature of 540 °C. For many applications, such as solar cells, where

the unwanted impurity level should be minimized, it is thus required to completely remove the unintentional sidewall growth.

Carrier lifetime and temperature-dependent PL-efficiency measurements were performed on both WZ and sidewall-removed ZB TSL NWs from 4 K up to room temperature. At low temperature (4 K) and at a very low excitation power of 64 nJ pulse^{-1} cm^{-2}, a nearly intrinsic exciton lifetime [39] of 0.97 ns in WZ and 0.82 ns in ZB is observed without using surface passivation or employing a core–shell design (see inset of figure 4). The observed exciton lifetime at low temperature increases to 2.4 ns in WZ and 2.8 ns in ZB with an excitation power up to 21 μJ pulse^{-1} cm^{-2} (see supporting information available at stacks.iop.org/Nano/24/115705/mmedia), which is typical for a NW in which radiative exciton recombination is the dominant recombination process [24, 28]. Our lifetimes at very low excitation power are somewhat higher than in [28], but lower than in GaAs/AlGaAs core/shell NWs [39], however, we emphasize that these low-temperature lifetimes are probably more sensitive to the (NW diameter-dependent) local photonic density of states than being a genuine measure for the NW optical quality. At high temperature, the radiative lifetime decreases with $T^{-3/2}$, whereas nonradiative recombination increases with temperature. Rosenwaks *et al* has shown that the electron capture into neutral acceptors (e–A$^{(0)}$) is the dominant nonradiative recombination mechanism in p-doped bulk InP [36]. We expect that the strong suppression of the impurity incorporation into our NWs by using *in situ* etching and high-temperature growth will also strongly reduce the nonradiative e–A$^{(0)}$ recombination. We indeed observe that the PL efficiency only decreases by a factor of 17 and 35 for WZ and ZB TSL NWs, respectively, when we increase the temperature from 10 to 293 K (see supporting information available at stacks.iop.org/Nano/24/115705/mmedia). We emphasize that the resulting high PL efficiency at room temperature is realized in InP NWs without surface passivation and without a shell to protect the free NW surface.

4. Conclusions

We have studied the optical and structural properties of pure wurtzite and zincblende twinning superlattice InP NWs grown at a very high temperature of 540 °C. The pure wurtzite InP NWs are free of stacking faults and exhibit finely resolved bandgap-related transitions with a free exciton line at 1.491 eV and an impurity bound exciton line 5.5 meV lower. The zincblende twinning superlattice InP NWs contain a considerable amount of impurities in the VS-grown sidewall. This contaminated sidewall can be almost completely eliminated by simple chemical etching, resulting in a high-quality core which was axially grown by the vapor–liquid–solid mechanism. Both types of NWs exhibit long carrier lifetimes and high PL efficiencies up to room temperature, thus showing great potential for NW devices.

Acknowledgments

We acknowledge the long-term energy and innovation program EOS-LT, which is funded by Agentschap NL, as well as the Cobra research school funded by NWO. The research leading to these results has also received funding from the European Union Seventh Framework Programme under grant agreement No. 265073.

References

[1] Nadj-Perge S, Frolov S M, Bakkers E P A M and Kouwenhoven L P 2010 *Nature* **468** 1084–7
[2] Hu Y, Kuemmeth F, Lieber C M and Marcus C M 2012 *Nature Nanotechnology* **7** 47–50
[3] Mourik V, Zuo K, Frolov S M, Plissard S R, Bakkers E P A M and Kouwenhoven L P 2012 *Science* **336** 1003–7
[4] Bulgarini G, Reimer M E, Hocevar M, Bakkers E P A M, Kouwenhoven L P and Zwiller V 2012 *Nature Photon.* **6** 455–8
[5] Kayes B M, Atwater H A and Lewis N S J 2005 *Appl. Phys.* **97** 114302
[6] Tian B, Zheng X, Kempa T J, Fang Y, Yu N, Yu G, Huang J and Lieber C M 2007 *Nature* **449** 885–9
[7] Heurlin M, Wickert P, Fält S, Borgström M T, Deppert K, Samuelson L and Magnusson M H 2011 *Nano Lett.* **11** 2028–31
[8] Borgström M T, Wallentin J, Heurlin M, Fält S, Wickert P, Leene J, Magnusson M H, Deppert K and Samuelson L 2011 *IEEE J. Sel. Top. Quantum Electron.* **17** 1050
[9] Mattila M, Hakkarainen T, Mulot M and Lipsanen H 2006 *Nanotechnology* **17** 1580–3
[10] Mishra A *et al* 2007 *Appl. Phys. Lett.* **91** 263104
[11] Tuin G, Borgström M, Tragardh J, Ek M, Wallenberg L, Samuelson L and Pistol M-E 2011 *Nano Res.* **4** 159–63
[12] Fang Z M, Ma K Y, Cohen R M and Stringfellow G B 1991 *Appl. Phys. Lett.* **59** 1446
[13] Borgström M T, Wallentin J, Tragardh J, Ramvall P, Ek M, Wallenberg L R, Samuelson L and Deppert K 2010 *Nano Res.* **3** 264–70
[14] Bao J M, Bell D C, Capasso F, Wagner J B, Mårtensson T, Trägårdh J and Samuelson L 2008 *Nano Lett.* **8** 836–41
[15] Wallentin J, Ek M, Wallenberg L R, Samuelson L and Borgström M T 2011 *Nano Lett.* **12** 151–5
[16] Stiles M D and Hamann D R 1990 *Phys. Rev.* B **41** 5280–2
[17] Stiles M D and Hamann D R 1988 *Phys. Rev.* B **38** 2021–37
[18] Joyce H J, Wong-Leung J, Gao Q, Tan H H and Jagadish C 2010 *Nano Lett.* **10** 908–15
[19] Shtrikman H, Popovitz-Biro R, Kretinin A, Houben L, Heiblum M, Bukała M, Galicka M, Buczko R and Kacman P 2009 *Nano Lett.* **9** 1506–10
[20] Algra R E, Verheijen M A, Borgström M T, Feiner L F, Immink G, van Enckevort W J P, Vlieg E and Bakkers E P A M 2008 *Nature* **456** 369–72
[21] Heiss M *et al* 2011 *Phys. Rev.* B **83** 045303
[22] Fry K L, Kuo C P, Larsen C A, Cohen R M, Stringfellow G B and Melas A 1986 *J. Electron. Mater.* **15** 91–6
[23] Caroff P, Dick K A, Johansson J, Messing M E, Deppert K and Samuelson L 2009 *Nature Nanotechnology* **4** 50–5
[24] Joyce H J *et al* 2012 *Nano Lett.* **12** 5325–30
[25] Dalacu D, Mnaymneh K, Lapointe J, Wu X, Poole P J, Bulgarini G, Zwiller V and Reimer M E 2012 *Nano Lett.* **12** 5919–23

[26] Naji K, Dumont H, Saint-Girons G, Penuelas J, Patriarche G, Hocevar M, Zwiller V and Gendrya M 2012 *J. Cryst. Growth* **343** 101–4
[27] Gadret E G *et al* 2010 *Phys. Rev.* B **82** 125327
[28] Chauvin N, Alouane M H H, Anufriev R, Khmissi H, Naji K, Patriarche G, Bru-Chevallier C and Gendry M 2012 *Appl. Phys. Lett.* **100** 011906
[29] Alouane M H H, Chauvin N, Khmissi H, Naji K, Ilahi B, Maaref H, Patriarche G, Gendry M and Bru-Chevallier C 2013 *Nanotechnology* **24** 035704
[30] Akopian N, Patriarche G, Liu L, Harmand J C and Zwiller V 2010 *Nano Lett.* **10** 1198
[31] Dean P J and Skolnick M S 1983 *J. Appl. Phys.* **54** 346
[32] Titova L V *et al* 2007 *Nano Lett.* **7** 3383
[33] Smith L M, Jackson H E, Yarrison-Rice J M and Jagadish C 2010 *Semicond. Sci. Technol.* **25** 024010
[34] Pemasiri K *et al* 2009 *Nano Lett.* **9** 648–54
[35] Perera S, Pemasiri K, Fickenscher M A, Jackson H E, Smith L, Yarrison-Rice M J, Paiman S, Gao Q, Tan H H and Jagadish C 2010 *Appl. Phys. Lett.* **97** 023106
[36] Rosenwaks Y, Tsimberova I, Gero H and Molotskii M 2003 *Phys. Rev.* B **68** 115210
[37] Zhang L, Luo J, Zunger A, Akopian N, Zwiller V and Harmand J-C 2010 *Nano Lett.* **10** 4055–60
[38] Xu T, Dick K A, Plissard S, Nguyen T H, Makoudi Y, Berthe M, Nys J-P, Wallart X, Grandidier B and Caroff P 2012 *Nanotechnology* **23** 095702
[39] Perera S *et al* 2008 *Appl. Phys. Lett.* **93** 053110